Draft version July 24, 2010
Preprint typeset using LaTeX style emulateapj v. 03/07/07

FORMATION EPOCHS, STAR FORMATION HISTORIES AND SIZES OF MASSIVE EARLY-TYPE GALAXIES IN CLUSTER AND FIELD ENVIRONMENTS AT Z=1.2: INSIGHTS FROM THE REST-FRAME UV

Alessandro Rettura[1], P. Rosati[2], M. Nonino[3], R. A. E. Fosbury[4], R. Gobat[2], N. Menci[5], V. Strazzullo[6], S. Mei[7], R. Demarco[1], H. C. Ford[1]

Draft version July 24, 2010

ABSTRACT

We derive stellar masses, ages and star formation histories of massive early-type galaxies in the z=1.237 RDCS1252.9-2927 cluster and compare them with those measured in a similarly mass-selected sample of field contemporaries drawn from the GOODS South Field. Robust estimates of these parameters are obtained by comparing a large grid of composite stellar population models with 8-9 band photometry in the rest-frame NUV, optical and IR, thus sampling the entire relevant domain of emission of the different stellar populations. Additionally, we present new, deep U-band photometry of both fields, giving access to the critical FUV rest-frame, in order to constrain empirically the dependence on the environment of the most recent star formation processes. We also analyze the morphological properties of both samples to examine the dependence of their scaling relations on their mass and environment. We find that early-type galaxies, both in the cluster and in the field, show analogous optical morphologies, follow comparable mass vs. size relation, have congruent average surface stellar mass densities and lie on the same Kormendy relation. We also that a fraction of early-type galaxies in the field employ longer timescales, τ, to assemble their mass than their cluster contemporaries. Hence we conclude that, while the formation epoch of early-type only depends on their mass, the environment does regulate the timescales of their star formation histories. Our deep U-band imaging strongly supports this conclusions. I shows that cluster galaxies are at least 0.5 mag fainter than their field contemporaries of similar mass and optical-to-infrared colors, implying that the last episode of star formation must have happened more recently in the field than in the cluster.

Subject headings: galaxies: clusters: individual: RDCS1252.9-2927 — galaxies: high-redshift — galaxies: fundamental parameters — galaxies: evolution — galaxies: formation — galaxies: elliptical — cosmology: observations

1. INTRODUCTION

The description of galaxy formation and evolution becomes far more complicated if one considers that a galaxy is not an isolated island universe. Many observations have shown that galaxies are in fact parts of groups, clusters and super-clusters, and that their properties are correlated with the environment in which they live. Several authors have shown that the local and the large-scale environments play an important role in determining many galaxy properties, such as star formation rate, gas content and morphology (Kodama & Bower 2001; Balogh et al. 2002). Several mechanisms have been proposed by theorists to account for these effects, such as ram pressure stripping, mergers and tidal effects (Gunn & Gott 1972; Dressler et al. 1997; Moore et al. 1996, 1998, 1999).

More than half of all stars in the local Universe are found in massive spheroids (e.g., Bell et al. (2003)). To derive the assembly history of the bulk of the stellar mass in the Universe it is thus fundamental to understand how and when the early-type galaxies (hereafter, ETGs) built up their mass. Several studies at $1 < z < 1.5$ indicate that the most massive galaxies in the field ($M_{stars} > 10^{11} M\odot$) may also be the oldest at a given epoch (Cimatti et al. 2004; Fontana et al. 2004; Saracco et al. 2004; Treu et al. 2005; Juneau et al. 2005; Tanaka et al. 2005). Other studies have shown that the massive early-type cluster galaxies have evolved mainly passively since $z \sim 1.0$ and that, since then, field galaxies have evolved as slowly as cluster galaxies (Bernardi et al. 1998; van Dokkum & Franx 1996; van Dokkum & Franx 2001; Treu et al. 1999, 2001; Kochanek et al. 2000; van Dokkum & Stanford 2003; Strazzullo et al. 2006; De Propris et al. 2007). These studies imply an epoch of massive early-type galaxy formation at redshifts well beyond $z = 2$. At earlier epochs, an abundance of dusty and star forming galaxies are found, which appear to be the progenitors of massive ETG (Adelberger et al. 2005). Contrary to what is observed in low redshift clusters, observations of $z > 2$ proto-clusters have shown that the quiescent red sequence, which traces the passively evolving ellipticals, has yet to appear (Kurk et al. 2004). This supports a paradigm where a more rapid evolution in denser environments is occurring a $z \sim 2$. More recent studies (Kodama et al. 2007; Zirm et al. 2008) reveal the appearance of the red sequence of galaxies by $2 < z < 3$,

[1] Department of Physics and Astronomy, Johns Hopkins University, Baltimore, MD, USA
[2] ESO - European Southern Observatory, Garching bei Muenchen, D- 85748, Germany
[3] INAF - Osservatorio Astronomico di Trieste, via G.B. Tiepolo 11, 34131 Trieste, Italy
[4] ST-ECF - Karl Schwarzschild straase, 2, Garching bei Muenchen, D- 85748, Germany
[5] INAF - Osservatorio Astronomico di Roma, via di Frascati 33, I-00040, Monteporzio, Italy
[6] National Radio Astronomy Observatory, P.O. Box O, Socorro, NM 87801.
[7] GEPI, Observatoire de Paris, Section de Meudon, Meudon Cedex, France

although with a large scatter.

Thus, galaxy cluster samples at $1.0 < z < 2.0$ provide a key link to the more active epoch at $z > 2$ where proto-clusters around powerful high redshift radio galaxies are not yet populated by passively evolving ETG (Kurk et al. 2004). Cluster galaxies have evolved and were more luminous and bluer at high redshift (e.g. van Dokkum et al. (1998)). Other observational results, e.g. Labbé et al. (2005), Papovich et al. (2006), Kriek et al. (2006), suggest that by $z \sim 2$ we are entering the star formation epoch of massive ETGs, leading us to ask whether the properties of ETG at intermediate redshift are consistent with this interpretation. On the basis of these studies, the evidence seems not only to indicate an epoch of massive early-type galaxy formation at $z > 2$ but also that in the range $1.0 < z < 2$, the environmental effects start to become more substantial.

In fact, the most distant clusters known to date (all at $z < 1.5$) provide the strongest test of model predictions. Relevant investigations include the observation of the aftermath of an off-axis merger in XMMXCS2215.9-1738 (Hilton et al. 2007) at z=1.45, a tight red sequence of ETG at $0.8 < z < 1.3$ (Rosati et al. 2004; Blakeslee et al. 2003; Blakeslee et al. 2006; Lidman et al. 2004; Mei et al. 2006a,b), a slowly evolving K-band luminosity function at odds with hierarchical merging scenarios (Toft et al. 2004; Strazzullo et al. 2006), and a tight and slowly evolving Fundamental Plane (hereafter, FP) out to z=1.25 (Holden et al. 2005) have been found. Intriguingly, Steidel et al. (2005) have found that galaxies in a proto-cluster environment at $z = 2.3$ have mean stellar masses and inferred ages that are ~ 2 times larger than identically selected galaxies outside of the structure.

A long-standing prediction of hierarchical models is that ETG in the field are younger for a given mass than those in cluster cores, since galaxy formation is accelerated in dense environments (Diaferio et al. 2001; De Lucia et al. 2004). Studies at low redshift, using chemical abundance indicators (Bernardi et al. 2006) or the analysis of fossil record data via line strength indices (Thomas et al. 2005; Clemens et al. 2006; Sánchez-Blázquez et al. 2006) suggest that star formation in low density environments was delayed by 1-2 Gyr. FP studies at $z \simeq 1$ have shown that massive ETG in the field and in clusters ($M_* > 3 \cdot 10^{10} M_\odot$) share the same FP evolution (M/L vs. z) and have approximately similar ages (within ~ 0.4 Gyr) and star formation histories (e.g., van Dokkum & van der Marel (2007), di Serego Alighieri et al. (2006)). FP studies have also shown that M/L ratios of massive cluster and field ETG evolve slowly and regularly and that there is evidence that low-mass galaxies evolve faster than high-mass galaxies (e.g, Holden et al. (2005); Jørgensen et al. (2006); Treu et al. (2005); van der Wel et al. (2005); di Serego Alighieri et al. (2005)). This so-called *downsizing* effect is at odds with earlier semi-analytic model predictions (Baugh et al. 1996; Kauffmann & Charlot 1998; Somerville et al. 2004) (see also Renzini (2006)), although it can be reconciled in the most recent versions based on ΛCDM cosmogony (De Lucia et al. 2006) and assuming that dry-mergers between non star-forming ETG may occur and build up the massive early-type galaxy population (Khochfar & Burkert 2003; Bell et al. 2005).

The majority of the above mentioned studies have focused on rest-frame optical and/or infrared spectrophotometric data. However, the optical spectrum remains largely unaffected by moderate amounts of past or recent star formation. More recently, deep optical surveys (e.g. FIRES (Franx et al. 2003), GOODS (Giavalisco et al. 2004), COMBO-17 (Wolf et al. 2004), MUSYC (Gawiser et al. 2006)) have provided access to the rest-frame UV spectrum beyond $z \sim 0.5$, enabling more in-depth studies of the ETG population. Studies of local ETG have revealed the existence of relatively young stellar populations. Such fossil record observations of absorption line-strengths (Trager et al. 2000; Thomas et al. 2004) find that stellar populations younger than $\sim$ 5Gyr (i.e. which must have formed between $z \sim 1$ and the present-day) are common in ETGs. Furthermore, a significant fraction of $z \leq 0.1$ ETG show relatively blue NUV-optical colors (Kaviraj et al. 2005), within extended disks (Kauffmann et al. 2007), indicating star-formation over the past Gyr. The inferred recent star-formation amounts to only $\sim 1\%$ of the total stellar mass. In a more recent study, Kaviraj et al. (2007) have also shown that a significant fraction of $0.5 < z < 1.0$ ETG show relatively blue NUV colors, indicating star-formation over the past 1 Gyr. At slightly higher redshift, spectroscopic studies at $z \sim 1.2$ have shown that both the brightest ETG of RDCS1252.9-2927 (Demarco et al. 2007) and the massive ETG in the GDDS fields (Le Borgne et al. 2006) show evidence for recent (i.e., within 1Gyr) star-formation on the basis of prominent post-starburst features in galaxy spectra (e.g., H_δ absorption line).

However, since little is known about the dependence on the environment of the recent star-formation rates (hereafter, SFR) in ETG at $z \simeq 1.2$, in this work, we complement our modeling of galaxy Spectral Energy Distributions (hereafter, SEDs), from NUV to NIR, presenting result of deep observations of ETG in cluster and field obtained with *VLT*/VIMOS in the U-band filter, that directly probes the FUV regime at the redshift of our samples, as shown in Fig 1.

By studying stellar population ages at $z = 1.2$, we provide a key test of the paradigm of an accelerated evolution in the highest density environments. For galaxies observed at $z \leq 1$ most of their difference could have been smoothed out by billion years of mostly passive evolution. By comparing stellar masses, ages and inferred star formation histories of cluster ellipticals with their field contemporaries, we directly test the prediction that the cluster environment should display accelerated evolution, resulting in larger masses and ages.

The primary observational goal of this work is to use *HST*/ACS in the rest-frame Near-UV (hereafter, NUV) and optical[8],and *VLT*/ISAAC, *Spitzer*/IRAC in the rest-frame near-IR (hereafter, NIR)[9] to measure stellar population ages and masses for ETG in the z=1.237 RDCS1252.9-2927 cluster (Rosati et al. 2004) and compare them to those measured on similarly selected sample of field contemporaries drawn from the GOODS South

[8] wavelength ranges which are known to be stellar population age sensitive

[9] a wavelength range which is known to be strongly correlated with the underlying stellar mass (Gavazzi et al. 1996)

Field. This allows us to directly analyze the entire relevant spectral energy distribution of the different stellar populations, enabling us to improve constraints on galaxy ages, masses and star formation histories in both environments at $z \simeq 1.2$.

We note that in an accompanying paper, Gobat et al. (2008), we also compare the coadded spectroscopic information available on both samples of ETG with a large grid of composite stellar population models.

We also analyze the morphological properties of ETG in the field and in the cluster. By studying scaling relations in this relevant redshift range we can trace back where the majority of stars formed as a function of the environment and stellar mass.

The structure of this paper is as follows. The description of our data-sets, cataloging and sample selection is described in §2. In §3 we describe our methods in deriving galaxy sizes and morphologies as well as inferring ages and masses from stellar population analysis. The results of our study are discussed in §4, while in § 5 we summarize our conclusions.

We assume a $\Omega_\Lambda = 0.73$, $\Omega_m = 0.27$ and $H_0 = 71$ km $\cdot$ s^{-1} $\cdot$ Mpc^{-1} flat universe (Spergel et al. 2003), and use magnitudes in the AB system throughout this work.

2. DESCRIPTION OF THE DATA

This work is based on spectroscopic and photometric data of two fields which have extensive spectral coverage over the wavelength range $0.4 - 8\mu$m: the Chandra Deep Field South (hereafter, CDFS) observed by the Great Observatories Origin Deep Survey (GOODS, (Giavalisco et al. 2004)) and the field around the X-ray luminous cluster RDCS1252.9-2927 at $z = 1.237$ (hereafter CL1252; Rosati et al. 2004).

The archival data for the CDFS comprise deep imaging in 8 bands, *HST*/ACS (B_{F435W}, V_{F606W}, i_{775W}, z_{F850LP}) (Giavalisco et al. 2004), *VLT*/ISAAC, (J,K_s) (Retzlaff et al., in prep.), *Spitzer*/IRAC ($3.6\mu m$, $4.5\mu m$) [10], as well as spectroscopic data taken with *VLT*/FORS2 300I grism by the ESO-GOODS survey (Vanzella et al. 2005, 2006) and the K20 survey (Cimatti et al. 2002).

The archival data for CL1252 consist of deep imaging in 9 bands, *VLT*/FORS2 (B, V, R), *HST*/ACS (i_{F775W},z_{F850lp}) (Blakeslee et al. 2003), *VLT*/ISAAC (J_s,K_s) (Lidman et al. 2004), *Spitzer*/IRAC ($3.6\mu m$, $4.5\mu m$), as well as spectroscopic data taken with *VLT*/FORS2 and already published in Demarco et al. (2007).

2.1. *Cataloging of observations and sample selection*

This work builds on the analysis performed on the same data-sets by Rettura et al. (2006), where photometric-stellar (hereafter, simply *stellar*) masses and dynamical masses of $z \sim 1$ ETG with known velocity dispersion measurements were analyzed for both the CDFS and CL1252. We refer to the above mentioned paper for more details about data reduction and cataloging (e.g., photometrical errors, PSF-matched photometry).

The resulting data-sets for the cluster and the field have homogeneous depths and wavelength coverage, allowing the application of similar selection criteria for both samples. The data allow the reconstruction of galaxy SED by sampling the entire relevant spectrum range emitted by all the different stellar populations. As is shown in Fig 1, our SED-fitting analysis is based on data from the NUV rest-frame (B-band observations are centered at $\lambda \sim 2000$Å at z$\simeq$ 1.2) through the NIR (IRAC/4.5μm imaging probes the $\sim 2\mu m$ rest-frame at the redshift of CL1252).

The availability of 8 to 9 passbands spanning such a large wavelength range enables the estimate of accurate stellar masses of ETGs (Rettura et al. 2006) and makes it possible to compare stellar population properties of homogeneously selected samples of ETG in both environments. In addition, high quality *HST*/ACS z_{F850LP}-band imaging enables the study of their morphologies in great detail.

Throughout this work, we compare morphological and stellar population properties of cluster galaxies with those shown by a sample of *field contemporaries* drawn from the spectroscopic surveys in the redshift range $z = 1.237 \pm 0.15$. Although photometric-redshift selected samples are widely employed in the literature, we do not favor this approach, as we believe it may result in the pollution of the samples by a large fraction of redshift outliers, which could adversily affect our conclusions.

The depth of the *VLT*/ISAAC images and the extended multi-wavelength data for both fields allows us to define complete mass-selected samples. In an accompanying paper, Gobat et al. (2008), we study the relative photometric and spectroscopic completeness of our CDFS and CL1252 mass-selected samples. The reader is referred to that paper for more details. Here, we note that photometric completeness is obtained if we limit our analysis to stellar masses larger than $M_{lim} = 5 \cdot 10^{10} M_\odot$.

A selection of CL1252 ETG along the cluster red-sequence is efficiently provided by a color selection of $i_{775} - z_{850} > 0.8$ (Blakeslee et al. 2003). In the spectroscopic sample of Demarco et al. (2007) there are 22 red sequence galaxies ($i_{775} - z_{850} > 0.8$) with $M_* > M_{lim}$, of which 18 are classified as passive ETGs, with no emission line in their observed spectra. For the corresponding CDFS field sample, the same criteria yield 27 ETG in CDFS with FORS2 spectra giving redshift in the range $z = 1.237 \pm 0.15$. From visual morphological analysis, following the classification scheme of Blakeslee et al. (2003), the vast majority of the selected ETG also have typical elliptical or lenticular morphologies

Comparing, as a function of stellar mass, each spectroscopic sample with its corresponding photometric-redshift sample (see Fig.1 and Table 1 of Gobat et al. (2008)) we find that the spectroscopic follow-up for CL1252 is more complete at the low mass end (reaching a $\sim 60\%$ completeness by $M_* = M_{lim}$) than in CDFS (reaching a 60% completeness only by $M_* \simeq 2 \cdot 10^{11} M_\odot$). Thus our sample of ETG in CDFS is likely to be more incomplete at the low mass end than the CL1252 one. We will return to this point when discussing our results in §4.2.

2.2. *VIMOS U-band photometry of CDFS and RDCS1252.9-2927 fields.*

[10] CDFS imaging and spectroscopic data are publicly available through the GOODS collaboration web-site: http://www.stsci.edu/science/goods/.

The new observations with *VLT*/VIMOS in the *U*-band allow us to directly study the FUV rest-frame emission, which is very sensitive to recent star formation. This allows us to constrain the instantaneous and recent star-formation in massive ETG as a function of their environment.

The reader is referred to Nonino et al. (2008) for more details on data reduction and cataloging. These surveys provide deep *U*-band imaging in the CDFS for a total integration time of ∼15h, to AB depths of U= 28.27 mag (3σ, 1" radius aperture), and in the cluster region for a total integration time of ∼2.5h, to AB depth of U=27.3 mag. We note that the ∼1 mag difference in depth between the two data-sets is not only due to the difference in the total allocated time, but also to the larger galactic extinction at the location of the CL1252 cluster ($A(V) = 0.247$, compared to the one at the CDFS location, $A(V) = 0.026$). Assuming an extinction following the Cardelli et al. (1988) relation, we estimate a dimming of ∼ 0.4 mag in the VIMOS *U*-band for CL1252 with respect to CDFS.

The VIMOS U-band filter has a colour term with respect to standard Johnson U-band filter. However this term has been set to zero both in CL1252 and CDFS fields in the process of catalog creation, thus placing the reported magnitudes in the VIMOS-U system.

3. DATA ANALYSIS

3.1. *Derivation of Galaxy Sizes and Morphologies*

To find structural differences shown by ETG of the same mass in different environments we have to study their morphology in a more quantitative way than a simple visual analysis. One way is to model and compare their galaxy light distributions, which are known to correlate with galaxy type and dynamical state. We also measure and compare galaxy sizes as a function of their mass, to obtain information on the physical scale of the potential well in which the stellar mass is assembled.

We have used GIM2D, a fitting algorithm for parameterized two-dimensional modeling of surface brightness (SB) distribution (Simard 1998; Marleau & Simard 1998), to fit each galaxy light distribution by adopting a simple Sérsic (1968) profile of the form:

$$I(r) = I_{e_n} \cdot 10^{-b_n[(r/R_{e,n})^{1/n}-1]}, \quad (1)$$

where $b_n = 1.99n - 0.33$ (Capaccioli 1989), and $R_{e,n}$ is the effective radius (i.e., the projected radius enclosing half of the light). The classical de Vaucouleurs profile thus simply corresponds to a Sérsic index $n = 4$ and $b_n = 7.67$ in Eq. 1. In this work, we allow n to span the range between 0 and 5.

GIM2D performs a profile fit by deconvolving the data with the point spread function. We model PSFs with analytic functions from visually selected stars in the surrounding ($30'' \times 30''$) region of each galaxy. We model a different PSF for each region in order to account of PSF variations with the position in the field. A 2D radial multi-gaussian function has been fitted simultaneously to tens of selected stars around the galaxies of our sample with outputs being stacked together to create a single PSF image for each region. The reader is referred to Rettura et al. (2006) for more details on our method for modeling galaxy PSFs and SB profiles from *HST*/ACS images. Here we also note that using PSF constructed with distortion-corrected Tiny Tim (Krist 1995) models results in negligible differences (see, e.g., van der Wel et al. (2005), Treu et al. (2005)).

The result of the bidimensional fit is the semi-major axis a_e of the projected elliptical isophote containing half of the total light, the axis ratio b/a and the Sérsic index n, which we have left as free parameters. The effective radius is computed from $R_e = a_e\sqrt{b/a}$. The average surface brightness within the effective radius (in mag/arcsec^2) is obtained from the absolute magnitude M:

$$\langle\mu\rangle_e = M + 5logR_e + 38.567, \quad (2)$$

with R_e in kiloparsec. In order to obtain the morphological parameters in the rest-frame *B*-band, which is customary in morphological studies, we have used the *HST*/ACS images taken with the F850LP filter, since these are very close to the *B*-band at the redshift of our galaxies for both the cluster and the field samples.

3.2. *Derivation of stellar masses and star-formation weighted ages*

Adopting a similar approach to Rettura et al. (2006), we derive stellar masses and ages for each galaxy in our samples using multi-wavelength PSF-matched aperture photometry from 8 and 9 passbands for the CDFS and CL1252 fields respectively, from observed *B*-band to observed $4.5\mu m$. For each galaxy, we compare the observed SED with a set of composite stellar populations (hereafter, CSP) templates computed with models built with Bruzual & Charlot (2003) models, assuming solar metallicity, Salpeter (1955) Initial Mass Function (hereafter, IMF) and dust-free models. In Rettura et al. (2006) we did investigate the effect of dust extinction on the best-fit stellar masses by including a fourth free parameter, $0.0 < E(B-V) < 0.4$, following the Cardelli et al. (1989) prescription. By performing the fit on 28 ETG at $z \sim 1$, we found that in ∼ 40% of the cases $E(B-V) = 0$ gives the best fit. In the remaining cases, masses which are lower by 0.2 ± 0.1 dex are found, with corresponding $E(B-V) \leq 0.2$. This test supports the validity of the dust-free model assumption.

For our CSP models, we assume the following grid of exponentially-declining star formation history (SFH) scenarios, $\Psi(T - t', \tau)$:

$$\Psi(T - t', \tau) = e^{-\frac{T-t'}{\tau}} \cdot \frac{M_\odot}{yr}, \quad (3)$$

where $0.05 \leq \tau \leq 5$ Gyr, T is the cosmic time and $(T - t')$ is the age[11] of the stellar population model formed at time t' at a SFR, $\Psi(t')$.

In determining galaxy model ages, masses and star formation histories from SED fitting, is important to understand how much our estimates could possibly be affected by dust extinction, and "age-metallicity"[12] and "age-SFH" degeneracies.

Galaxies could appear redder as a result of any of, a shorter τ , a larger extinction, or an older age, would

[11] The range of acceptable ages for a given galaxy has been limited by the age of the universe at its observed redshift.

[12] We emply the working assumption that the most-massive ETG have all solar metallicities.

all transform a galaxy spectrum into a redder one. This effect is simply illustrated in the top panel of Fig. 2. We show the $i_{775} - K_s$ vs. $v_{606} - i_{775}$ color-color plot of BC03 CSP models at z=1.24 superimposed on our CDFS ETG sample observed colors. The squares show the various τ models predictions. The grids are drawn for seven different τ and five model ages (2, 2.5, 3, 3.5, 4 Gyrs): the colored lines represent iso-metallicity colors of solar metallicity, $Z_{\odot}$. It is evident from this figure that it might become very hard to distinguish different model parameters with SED fitting studies based on rest-frame optical and infrared photometry only (i.e., $\lambda_{rest} > 2700$ Å). However, as we show in Fig. 1, the use of information coming from the rest-frame UV is crucial to distinguish the different parameters of the stellar population modeling (e.g. ages and τ). As we demonstrate in the bottom panel of Fig. 2, by including available UV rest-frame photometry in the SED fits (B-band observed-frame[13]) we are able to break the "age-SFH degeneracy". Note that the rest-frame UV remains also largely unaffected by the "age-metallicity" degeneracy, which plagues optical studies (Worthey 1994). Hence the extensive panchromatic method we use maintains its age-sensitivity across a large range of masses, ages and τ, providing more reliable estimates of these parameters compared to those obtained using optical-to-infrared studies.

To account for the average age of the bulk of the stars in a galaxy, we refer throughout this paper to *star-formation weighted* ages, $\overline{t}$, defined as:

$$\overline{t}(T-t^{'},\tau) \equiv \frac{\int_0^T (T-t^{'})\Psi(T-t^{'},\tau)dt^{'}}{\int_0^T \Psi(T-t^{'},\tau)dt^{'}}. \qquad (4)$$

Assuming $\Psi(T-t^{'},\tau)$ as in Eq. 3 we obtain,

$$\overline{t} = \tau \cdot e^{-\frac{T-t^{'}}{\tau}} + (T-t^{'}) + \tau. \qquad (5)$$

By comparing each observed SED with these atlases of synthetic spectra, we construct a 3D χ^2 space spanning a wide range of star formation histories, model ages and masses. The galaxy mass in stars M_*, the τ and the inferred $\overline{t}$ of the models giving the lowest χ^2 are taken as the best-fit estimates of the galaxy stellar mass, age, and SFH timescale. We note that this procedure results in typical errors for galaxy ages of ~ 0.5Gyr, and for τ of $\sim 0.2Gyr$. Typical uncertainties on the mass determination are about $\sim 40\%$ (i.e., 0.15 dex) (Rettura et al. 2006).

The reliability of spectrum synthesis models at $\lambda_{obs} \sim 2\mu m$ has long been debated (Maraston (1998) and references therein). In the rest-frame NIR regime, in early stages of the galaxy evolution, a short-duration thermally pulsating (TP-) AGB phase is known to be relevant. In Rettura et al. (2006) we have shown that PEGASE.2 (Fioc & Rocca-Volmerange 1997), BC03, and Maraston models (hereafter M05; Maraston 2005) yield consistent stellar masses (within typical errors of 40%) for z$\sim$ 1 ETGs. Therefore we do not expect our stellar mass estimates to much depend on the actual stellar population synthesis model adopted. On the other hand, in §4.2 we discuss the effect on the galaxy ages of the use of other models such as M05.

[13] corresponding to $\sim$ 2000 Å at $z = 1.24$

In Fig. 3 we plot the stellar mass versus $U - B$ rest-frame color diagram of the mass-selected samples of CL1252 cluster early- (filled red circles) and late-type (red stars) galaxies as well as of CDFS field early- (filled blue circles) and late-type (blue stars) galaxies. The cluster ETG red sequence is evident, as well as the larger scatter in color of the field ETG around that sequence.

In Fig. 4 a similar diagram is compared with the predictions of the Menci et al. (2008) semi-analytical models for galaxies in clusters (defined as host Dark Matter haloes with $M > 10^{14} M_{\odot}$); the color code represents the abundance, normalized to the maximum value, of galaxies in a given $mass - (B-V)$ bin.

We note that the color and scatter of the sequence predicted by the models indicate that the existence of ETG confined to a narrow CMR by $z \approx 1.2$ is indeed consistent with predictions of hierarchical models including AGN feedback. However, the latter still yield a somewhat flatter slope of the CMR and an excess of red, low-mass galaxies. These discrepancies constitute a common feature of all hierarchical models, due to the following physical processes: i) the biasing effect, causing low-mass galaxies residing in high-density environment to collapse earlier; ii) the starbursts, present mainly at high-redshifts in biased density environments (like those originating the clusters), triggering early star formation at $z \gtrsim 2$; iii) the "strangulation" effect, namely, the stripping of gas in galaxies with shallow potential wells (such gas is included in the intra-cluster medium). In fact, in hierarchical models, low-mass galaxies are the main cause of the larger fraction of red objects characterizing the galaxy population in high-density environments.

4. RESULTS AND DISCUSSION

4.1. *The dependence of ETG scaling relations on environment*

The FP is known to be a powerful tool for studying the evolution of ETGs (Djorgovski & Davis 1987). In as similar way to the small scatter of the color-magnitude relation (Bower et al. 1992), the tightness of the FP (Jorgensen et al. 1996; Bernardi et al. 2003) constrains the homogeneity of the ETG stellar population. Because of its dependence on galaxy luminosity, the FP is sensitive to recent star formation episodes.

One of its projections shows a tight relation between the effective radius, R_e, and the mean surface brightness $< \mu_e >$ measured inside R_e, also known as the Kormendy (1977, hereafter KR) relation:

$$< \mu_e >= \alpha + \beta log(R_e), \qquad (6)$$

where the slope $\beta \simeq 3$ is found to be costant out to $z \simeq 0.65$ (La Barbera et al. 2003), while the value of α depends on the photometric band adopted to derive the structural parameters. Here we adopt the KR as one of the tools for investigating the structural properties of ETG with the aim of understanding the role of the environment in shaping ETG of similar masses and optical-to-infrared colors.

In Fig. 5, we find very similar KRs for the two samples. Both the derived zero points and slopes are consistent within the errors. These relations show that at the effective radius, large (massive) galaxies are fainter than small galaxies regardless of the environment. This in turn indicates that large galaxies are less dense than

small galaxies in both the cluster and field at $z \simeq 1.2$. For comparison, we overplot the KR at $z \sim 0$ found by La Barbera et al. (2003) (dotted-dashed red line), K-corrected to our rest-frame B-band. Our galaxies are brighter by 1-2mag than at low redshift, a discrepancy that other studies at $1.0 \lesssim z \lesssim 1.4$ have also found difficult to explain with the assumption that galaxies undergo only a pure luminosity evolution with redshift (e.g., Longhetti et al. (2007)). In fact, our galaxies show an evolution of $< \mu_e >$ which exceeds ~ 2 times the one expected in the case of pure luminosity evolution ($\sim$ 1mag). According to Eq. 2, the other quantity affecting $< \mu_e >$ is the effective radius. Therefore to recover this discrepancy we can assume that, as a function of redshift, ETG undergo a size evolution as well: the effective radius of ETG should increase by at least factor ~ 1.5 from z$\simeq$ 1.2 to z$\sim$ 0 both in the cluster and in the field environment.

Recent studies of the dependence on environment of the size vs. stellar mass relation (Trujillo et al. 2004; McIntosh et al. 2005; Trujillo et al. 2006, 2007) found that the bulk of galaxies with comparable stellar masses to ours were at least a factor 2 smaller at higher redshifts than locally. This is qualitatively consistent with the observed trend in our data, (see Fig. 6) when the sizes and masses our samples are compared with the local relation for ETG in SDSS (dotted-dashed red line; Shen et al. 2003). We find no-dependence on the environment of the R_e vs. M_* relation, implying that cluster and field ETGs must undergo similar luminosity and size evolution to match the typical values found for the ETG at lower redshifts. To explain how compact galaxies observed at $z > 1$ could possibly end-up on the local relation, a possible evolutionary mechanism that grows stellar mass and size has been suggested: a dissipationless ("dry") merging of gas-poor systems (e.g., (Ciotti & van Albada 2001; Nipoti et al. 2003; Khochfar & Burkert 2003; Boylan-Kolchin et al. 2006) that is efficient in increasing the size of the objects, while remaining inefficient at forming new stars.

In the local universe, the SFR per stellar mass (specific star-formation rate, SSFR) correlates strongly with galaxy concentration, effective radius and the average surface stellar mass density (σ_{50}; Kauffmann et al. 2003; Brinchmann et al. 2004). A striking similarity of cluster and field galaxies at $z \simeq$1.2 is again shown in Fig. 7 where we plot, σ_{50},

$$\sigma_{50} = \frac{0.5 M_\star}{\pi R_e^2}, \tag{7}$$

versus the stellar mass, and compare them with similar data in the literature drawn from Zirm et al. (2007) at $z \sim 2.5$. Quiescent Distant Red Galaxies (qDRGs) are drawn as red ellipses, star-forming DRGs (sDRGs) are drawn as open red stars, while blue stars indicates Lyman Break Galaxies (LBGs) from the same work. While some of our galaxies are almost as dense as the Zirm et al. (2007) and (Toft et al. 2007) quiescent distant red galaxies (qDRGs), both our samples (filled circles) overlap the region occupied by other $1.0 \lesssim z \lesssim 1.5$ galaxy samples (Trujillo et al. 2006; Daddi et al. 2005; van der Wel et al. 2006; Rettura et al. 2006) (open red squares, open red circles, open black circles, open black squares, respectively). As a comparison we also overplot the local relation for ETG in SDSS (red dotted-dashed line) calculated from the mass-size relation of Shen et al. (2003). It is very clear in Fig. 7 that the bulk of our galaxies in both samples have much larger densities that their local counterparts. To account for this effect in the context of a plausible formation scenario, semi-analytical modeling (e.g. Khochfar & Silk (2006)) suggests that ETGs formed in gas-rich mergers can result in very dense stellar cores, as the gas is driven to the center of this "wet" (dissipative) merger where it very efficiently produces massive starburts. Galaxies that merge in the early universe are likely to be gas-rich. Consequently the dense nature of this objects could be the result of much denser conditions of the universe at the time of their formation. We note that our finding that there is no dependence on the environment of the σ_{50} vs, M_* relation at z$\simeq$ 1.2 can provide an important datum for models of galaxy formation.

4.2. *The dependence of ETG ages and star formation histories on their environment*

As we apply the method described in section §3.2, we are able to directly compare the distribution of star-formation weighted ages in the field and in the cluster. As shown in the top panel of Fig. 8, we find the overall relative distribution of cluster and field ETG ages to be very similar. This result implies no significant delay in relative formation epochs is found for ETG in either environments. We find that $\sim 80\%$ of massive ETGs have ages in the range 3.5 ± 1.0 Gyr in both cluster and field.

To investigate the dependence of this result on the actual stellar population synthesis code adopted, we compare our current results (based on BC03 models) with those obtained with a set of similar dust-free CSPs templates built with Maraston (2005) models, adopting the same exponentially-declining SFHs of Eq. 3, and assuming solar metallicity and Salpeter (1955) IMF. The result of the analysis based on M05 models is shown in the bottom panel of Fig. 8 where we still find the cluster and field relative age distributions to be very similar, despite the fact that the contribution of the TP-AGB stars in these models are implemented in a different way. However, here we find that $\sim 60\%$ of galaxies have ages in the range 3.5 ± 1.0 Gyr; M05 models favor slightly younger ages ($\sim 1-2$ Gyrs) for $\sim$20% of ETG in both environments. This effect can be explained by the fact that, at about 1 Gyr, M05 models account for a larger amount of 2 μm flux than BC03 models of the same age, resulting in significantly redder color at younger ages, thus can favor $\overline{t} \sim$ 1-2Gyrs best-fits in a few cases.

To summarize, we find that, regardless of the actual stellar population synthesis code adopted, cluster galaxies ages have the same relative distribution as their field contemporaries: no significant delay in their formation epochs is found, within the errors ($\sim 0.5 Gyr$). This result is at variance with some versions of the hierarchical model of galaxy formation and evolution (Diaferio et al. 2001; De Lucia et al. 2006) and with fossil record studies (Thomas et al. 2005; Clemens et al. 2006), but in remarkably good agreement with the ones derived by van Dokkum & van der Marel (2007) and di Serego Alighieri et al. (2006) from the evolution of the M/L ratio. It should be noted that similar results are found by other works using independent methods and data-sets.

In the top-left panel of Fig. 9 we plot for both samples each galaxy age, $\overline{t}$, as a function of stellar mass. We note that the age of ETG increases with galaxy mass in all environments, which is in agreement with the so–called *downsizing* scenario of galaxy formation (Cowie et al. 1996). This effect can also be seen in the the top-right panel of Fig. 9, where we plot our galaxies' lookback time to formation as a function of their stellar mass, in both environments. Our result is in agreement with the one obtained with an independent method and data-set by (di Serego Alighieri et al. 2006) and based on z$\sim$ 1 ETG ages estimated from the FP parameters (see their Fig. 3).

Despite of the fact that cluster and field galaxy formation epochs are found to be similar, it could still be possible that the timescales of their SFH are significantly different. Firstly, the data show that the distribution of cluster and field optical colors is significantly different. As a function of the stellar mass, cluster galaxies are found to lie on a very tight red-sequence, while those in the field populate the color-sequence with a larger scatter (Fig. 3). Secondly, in Gobat et al. (2008) we find that the averaged spectrum of the cluster galaxies has a more pronounced 4000Å break than that of the field sample.

Both these pieces of observational evidence find a natural explanation in the framework of our modeling. As shown in the bottom-right panel of Fig. 9, as a function of stellar mass, we find that field ETG span a larger range of timescales than their cluster contemporaries, which are formed with the shortest τ at any given mass. According to our models, cluster ETG are found to have experienced more similar star-formation histories. As shown in the bottom-left panel of Fig. 9, cluster ETG form a color-age sequence with much smaller scatter than the field ones.

As discussed in §2.1, we recall that our field sample is more deficient in lower mass objects than the cluster sample because of the different depths of spectroscopic observations. However, even if the field sample were corrected for completeness, this would likely result in a larger fraction of field ETG at low mass, which are the ones that we found with longer τ. Hence this would amplify the difference between the typical timescales of the two samples, and so not affect our conclusions.

4.3. *The dependence of ETG FUV magnitudes on their environment*

The rest-frame FUV ($\sim \lambda$ 1700$\mathring{A}$) SED is a crucial range where hot ($> 9000K$), massive ($M > 2M_{\odot}$), short-living ($< 1Gyr$) stars emit most of their light. Thus it is a wavelength domain which is very sesnsitive to current or recent star formation. Most of the light from ETG is emitted in the optical and the NIR rest-frame. However, the FUV can be used as a good tracer of the residual current star-formation and to trace back, within the last Gyr, the most recent episode of star-formation. About 100Myr after star formation ceases, an ETG spectrum becomes dimmer and redder. Therefore, the fainter the rest-frame UV emission is, the earlier the star formation must have stopped. Over time, the galaxy spectrum fades and slowly reddens as the 4000 $\mathring{A}$ break becomes more pronounced. Here we have used the *VLT*/VIMOS U-band observations described in §2.2 to empirically constrain the dependence on the environment of the most recent star formation processes in z$\simeq$ 1.2 ETGs.

However, when analyzing UV rest-frame fluxes of massive ETG it is important to recall that core helium burning stars on the horizontal branch (HB) are known to produce a "UV upturn" feature (Yi et al. 1997, 1999). This effect can, in principle, complicate the disentanglement of the contributions to the UV spectrum of the evolved and young stellar populations. However, the onset of the HB typically takes 9 Gyr, meaning that, by z=1.2 (when the Universe is only 5Gyr old), not enough cosmic time has elapsed for this population of stars to appear. Hence the UV flux seen in our sample ETG must originate only from young stars.

In Fig. 10 we show U-band magnitudes (1" radius aperture; rest-frame $\sim 1700\mathring{A}$) as a function of stellar mass for the ETG detected in the field (filled blue circles). Solid lines represent the 1σ limit magnitudes of both data-sets (in blue for CDFS, in red CL1252). Dashed lines represent the 3σ limits. As already pointed out in §2.2, the combined effect of shorter total exposure times and higher galactic extinction at the location of CL1252, directly translates into a $\sim 1mag$ deeper U-band photometry for the CDFS.

A large fraction (75 %) of field ETG are ($> 3\sigma$) detected in the deep CDFS images. The observed magnitude of the median stack of these detections is U=27.46 mag (blue dotted line of Fig. 10), corresponding to a SFR=0.47 $M_{\odot}/yr$ (Sawicki & Thompson 2006). An image of the median U-band stack of the ETGs detected in the field, is displayed in the bottom-left corner of Fig. 10.

Since none of the CL1252 ETG is actually detected in our U-band data, we use their median stack, shown in the middle of Fig. 10, to provide a robust upper limit of $U > 27.3$ mag for the CL1252 early-type population, which corresponds to SFR$< 0.55M_{\odot}/yr$.

We note that the non detection of the CL1252 ETG cannot only be attributed to the shallower U-band data for the cluster. To prove this we have simulated how the CDFS detected ETG would appear in the 1252 data (more details can be found in Nonino et al. (2008)). We randomly placed the 20 U-band detected CDFS ETG (0.4 mag dimmed to match the relative difference in galactic extinction) in the CL1252 maximally exposed region, avoiding objects detected in the U-band, and repeated this step 30 times. Hence we generated 32 median stacks of 18 simulated galaxies each, picking up at random amongst the cutouts. Aperture photometry (1" radius) on these simulated *CDFS@1252* stacks results in a median value of U=27.8 mag which is in agreeement with the dimmed inputs of the simulations. In the bottom-right corner of Fig. 10 we show one of these stacks, which would be clearly detected in 1252. Comparing this last value to the upper limit we measured in the cluster data, we can state with confidence that cluster ETG are intrinsically fainter by at least 0.5 mag in the observed U-band than their field contemporaries of similar mass and optical-to-infrared colors.

This observational evidence corroborates the results of our stellar population synthesis analysis described in the previous subsection. In our proposed scenario, a generally shorter *timescale* of the star formation process among the cluster galaxy population would naturally result in a generally fainter observed U-band magnitudes

compared to the field population at z$\simeq$ 1.2.

5. CONCLUSIONS

We have obtained photometric parameters: PSF-matched aperture magnitudes in 9 bands from FUV to NIR rest-frame; and morphological information: effective radius, average surface brightness, Sérsic index and average surface stellar mass density for mass-selected samples of 45 cluster and field massive ($M > 5 \cdot 10^{10} M_{\odot}$) early-type galaxies at z$\simeq$ 1.2. Apart from a lower level of spectroscopic completeness for the least massive field galaxies, that we find not to affect our conclusions, our sample has the advantage of being photometrically complete at our mass limit and having galaxy types assigned spectroscopically.

For both samples we also have derived stellar masses, ages, and star formation histories, parameterized as timescales, τ, of exponentially declining CSP model templates built with BC03 and M05 models.

From the data analysis performed in this work, we have obtained the following results:

- Cluster and field ETG lie on a similarly tight Kormendy Relation at z$\simeq$ 1.2. When compared to the local relation, our galaxies are 1-2mag brighter than at z$\sim$0, similar to what has been found by other studies at $z \sim 1.0$ in the field (e.g., (Longhetti et al. 2007)). The evolution of the KR cannot be explained as pure luminosity evolution and we conclude that ETG must undergo a similar size evolution in both environments.

- We find no dependence on the environment of the *size vs. stellar mass* relation,or for the *average surface stellar mass density vs. stellar mass* relation at z$\simeq$ 1.2. As a comparison we constrast both of them with the local relations for ETG found in SDSS. We find that the bulk of our ETG in both samples have much smaller sizes (and larger densities) than their local counterparts. Our data therefore indicate a strong size evolution for both the cluster and field galaxies.

- We find no significant delay in the formation epochs of massive ETG observed in the cluster and in the field at z$\simeq$ 1.2. This result is true robust for models that treat the contribution of the TP-AGB stars in very differnt way (i.e., BC03 or M05). However our result is at variance with some versions of hierarchical models (Diaferio et al. 2001; De Lucia et al. 2006) and with fossil record studies (Thomas et al. 2005; Clemens et al. 2006), but is in remarkably good agreement with those obtained from the evolution of the M/L ratio.

- The age of ETG increase with galaxy mass in all environments, which is in agreement with the *downsizing* scenario. The site of active star formation must have shifted from the most massive to the less massive galaxies as a function of the cosmic time. The formation epochs of ETG only depends on their mass and not on the environment they live in.

- We present new deep U-band observations in the rest-frame FUV ($\sim \lambda$ 1700$\mathring{A}$) for both samples ETG. We detected 75 % of the field ETG at z$\simeq$ 1.2. The observed magnitude of the median stack of these detections is U=27.46 mag, which corresponds to a SFR=0.47 $M_{\odot}/yr$.

- None of the CL1252 ETG was actually detected in our shallower (by $\sim$ 1 mag) U-band data, but we used their median stack image to provide a robust upper limit of $U > 27.3$ mag for the CL1252 early-type population, which corresponds to SFR$<$ $0.55 M_{\odot}/yr$.

- Using simulations, we find that the median stack of the CDFS ETG could be clearly detected in the actual CL1252 data at U=27.8 mag. Comparing this value to the upper limit we measured from the cluster data, we can firmly state that cluster ETG are intrinsically fainter by at least 0.5 mag in the U-band than their field contemporaries of similar mass and optical-to-infrared colors. This observational evidence implies that the last episode of star formation must have happened more recently in the field than in the cluster.

- The data also show two other compelling pieces of evidence that cluster and field SFHs are significantly different: 1) as a function of the stellar mass, cluster galaxies are found to lie on a very tight color sequence while the field galaxies populate it with a larger scatter; 2) in a companion paper based on the same data-set, Gobat et al. (2008) find that the averaged spectrum of the cluster galaxies has a more pronounced 4000Å break than that of the field sample.

- Finally we have been also able to explain both these pieces of observational evidences in the framework of our stellar population modeling. Field ETG best-fit models span a larger range of timescales than their cluster contemporaries, which are formed with the shortest τ at any given mass.

While cluster and field galaxy observed at z$\simeq$ 1.2 form at approximately the same time, a high density environment is able to trigger more rapid and homogenous SFHs for the ETGs, limiting the range of possible star-formation processes. In low density environments, this effect must rapidly fade as ETG undergo a much broader range of possible star formation histories. We also note that this scenario is in very good agreement with the one proposed by Menci et al. (2008), based on the latest rendition of semi-analytic models.

A.R. is grateful to Roderik Overzier, Arjen van der Wel, and Loredana Vetere for useful discussions. A.R. is also grateful to Andrew Zirm for providing the data used in Fig. 7.

.

REFERENCES

Adelberger, K. L., Steidel, C. C., Pettini, M., Shapley, A. E., Reddy, N. A., & Erb, D. K. 2005, ApJ, 619, 697
Balogh, M. L., et al. 2002, ApJ, 566, 123
Baugh, C. M., Cole, S., & Frenk, C. S. 1996, MNRAS, 283, 1361
Bell, E. F., McIntosh, D. H., Katz, N., & Weinberg, M. D. 2003, ApJS, 149, 289
Bell, E. F., et al. 2005, ApJ, 625, 23
Bernardi, M., Renzini, A., da Costa, L. N., Wegner, G., Alonso, M. V., Pellegrini, P. S., Rité, C., & Willmer, C. N. A. 1998, ApJ, 508, L143
Bernardi, M., et al. 2003, AJ, 125, 1866
Bernardi, M., Nichol, R. C., Sheth, R. K., Miller, C. J., & Brinkmann, J. 2006, AJ, 131, 1288
Blakeslee, J. P., Franx, M., Postman, M., et al. 2003, ApJ, 596, L143
Blakeslee, J. P., et al. 2006, ApJ, 644, 30
Bower, R. G., Lucey, J. R., & Ellis, R. S. 1992, MNRAS, 254, 601
Boylan-Kolchin, M., Ma, C.-P., & Quataert, E. 2006, MNRAS, 369, 1081
Brinchmann, J., Charlot, S., White, S. D. M., Tremonti, C., Kauffmann, G., Heckman, T., & Brinkmann, J. 2004, MNRAS, 351, 1151
Bruzual, G. & Charlot, S. 2003, MNRAS, 344, 1000
Capaccioli, M. 1989, in World of Galaxies (Le Monde des Galaxies), 208–227
Cardelli, J. A., Clayton, G. C., & Mathis, J. S. 1988, ApJ, 329, L33
Cardelli, J. A., Clayton, G. C., & Mathis, J. S. 1989, ApJ, 345, 245
Cimatti, A., Pozzetti, L., Mignoli, M., et al. 2002, A&A, 391, L1
Cimatti, A., Daddi, E., Renzini, A., et al. 2004, Nature, 430, 184
Ciotti, L., & van Albada, T. S. 2001, ApJ, 552, L13
Clemens, M. S., Bressan, A., Nikolic, B., Alexander, P., Annibali, F., & Rampazzo, R. 2006, MNRAS, 370, 702
Cowie, L. L., Songaila, A., Hu, E. M., & Cohen, J. G. 1996, AJ, 112, 839
Daddi, E., et al. 2005, ApJ, 626, 680
De Lucia, G., Kauffmann, G., & White, S. D. M. 2004, MNRAS, 349, 1101
De Lucia, G., Springel, V., White, S. D. M., Croton, D., & Kauffmann, G. 2006, MNRAS, 366, 499
Demarco, R., et al. 2007, ApJ, 663, 164
Diaferio, A., Kauffmann, G., Balogh, M. L., White, S. D. M., Schade, D., & Ellingson, E. 2001, MNRAS, 323, 999
De Propris, R., Stanford, S. A., Eisenhardt, P. R., Holden, B. P., & Rosati, P. 2007, AJ, 133, 2209
di Serego Alighieri, S., Vernet, J., Cimatti, A., et al. 2005, A&A, 442, 125
di Serego Alighieri, S., Lanzoni, B., & Jørgensen, I. 2006, ApJ, 652, L145
Djorgovski, S. & Davis, M. 1987, ApJ, 313, 59
Dressler, A., et al. 1997, ApJ, 490, 577
Fioc, M. & Rocca-Volmerange, B. 1997, A&A, 326, 950
Fontana, A., Pozzetti, L., Donnarumma, I., et al. 2004, A&A, 424, 23
Franx, M., et al. 2003, ApJ, 587, L79
Gavazzi, G., Pierini, D., & Boselli, A. 1996, A&A, 312, 397
Gawiser, E., et al. 2006, ApJS, 162, 1
Giavalisco, M., Ferguson, H. C., Koekemoer, A. M., et al. 2004, ApJ, 600, L93
Gobat, R., Rosati, P., Strazzullo, V., Rettura, A., Demarco, R., & Nonino, M. 2008, A&A, submitted
Graham, A. W., & Guzmán, R. 2003, AJ, 125, 2936
Gunn, J. E., & Gott, J. R. I. 1972, ApJ, 176, 1
Jorgensen, I., Franx, M., & Kjaergaard, P. 1996, MNRAS, 280, 167
Jørgensen, I., Chiboucas, K., Flint, K., Bergmann, M., Barr, J., & Davies, R. 2006, ApJ, 639, L9
Juneau, S., et al. 2005, ApJ, 619, L135
Hilton, M., et al. 2007, ApJ, 670, 1000
Holden, B. P., van der Wel, A., Franx, M., et al. 2005, ApJ, 620, L83
Kauffmann, G., & Charlot, S. 1998, MNRAS, 294, 705
Kauffmann, G., Heckman, T. M., White, S. D. M., et al. 2003, MNRAS, 341, 54
Kauffmann, G., et al. 2007, ApJS, 173, 357
Kaviraj, S., Devriendt, J. E. G., Ferreras, I., & Yi, S. K. 2005, MNRAS, 360, 60
Kaviraj, S., et al. 2007, ArXiv e-prints, 709, arXiv:0709.0806
Kochanek, C. S., et al. 2000, ApJ, 543, 131
Khochfar, S., & Burkert, A. 2003, ApJ, 597, L117
Khochfar, S., & Silk, J. 2006, ApJ, 648, L21
Kodama, T., & Bower, R. G. 2001, MNRAS, 321, 18
Kodama, T., Tanaka, I., Kajisawa, M., Kurk, J., Venemans, B., De Breuck, C., Vernet, J., & Lidman, C. 2007, MNRAS, 377, 1717
Kormendy, J. 1977, ApJ, 218, 333
Kriek, M., et al. 2006, ApJ, 645, 44
Krist, J. 1995, Astronomical Data Analysis Software and Systems IV, 77, 349
Kurk, J. D., Pentericci, L., Röttgering, H. J. A., & Miley, G. K. 2004, A&A, 428, 793
La Barbera, F., Busarello, G., Merluzzi, P., Massarotti, M., & Capaccioli, M. 2003, ApJ, 595, 127
Le Borgne, D., et al. 2006, ApJ, 642, 48
Lidman, C., Rosati, P., Demarco, R., et al. 2004, A&A, 416, 829
Labbé, I., et al. 2005, ApJ, 624, L81
Longhetti, M., et al. 2007, MNRAS, 374, 614
Maraston, C. 1998, MNRAS, 300, 872
Maraston, C. 2005, MNRAS, 362, 799
Marleau, F. R. & Simard, L. 1998, ApJ, 507, 585
McIntosh, D. H., et al. 2005, ApJ, 632, 191
Mei, S., et al. 2006, ApJ, 644, 759
Mei, S., et al. 2006, ApJ, 639, 81
Menci, N., Rosati, P., Gobat, R., Strazzullo, V., Rettura, Mei, S., & Demarco, R. 2008, ApJ, submitted
Moore, B., Katz, N., Lake, G., Dressler, A., & Oemler, A. 1996, Nature, 379, 613
Moore, B., Lake, G., & Katz, N. 1998, ApJ, 495, 139
Moore, B., Ghigna, S., Governato, F., Lake, G., Quinn, T., Stadel, J., & Tozzi, P. 1999, ApJ, 524, L19
Nipoti, C., Londrillo, P., & Ciotti, L. 2003, MNRAS, 342, 501
Nonino, M., Rosati, Rettura, A. et al. 2008, in preparation
Papovich, C., et al. 2006, ApJ, 640, 92
Renzini, A. 2006, ARA&A, 44, 141
Rettura, A., et al. 2006, A&A, 458, 717
Rosati, P., Tozzi, P., Ettori, S., et al. 2004, AJ, 127, 230
Salpeter, E. E. 1955, ApJ, 121, 161
Sánchez-Blázquez, P., Gorgas, J., Cardiel, N., & González, J. J. 2006, A&A, 457, 809
Saracco, P., Longhetti, M., Giallongo, E., et al. 2004, A&A, 420, 125
Sawicki, M., & Thompson, D. 2006, ApJ, 642, 653
Sersic, J. L. 1968, Atlas de galaxias australes (Cordoba, Argentina: Obs. Astronomico, 1968)
Shen, S., Mo, H. J., White, S. D. M., Blanton, M. R., Kauffmann, G., Voges, W., Brinkmann, J., & Csabai, I. 2003, MNRAS, 343, 978
Simard, L. 1998, in ASP Conf. Ser. 145, 108–+
Somerville, R. S., Moustakas, L. A., Mobasher, B., et al. 2004, ApJ, 600, L135
Spergel, D. N., Verde, L., Peiris, H. V., et al. 2003, ApJS, 148, 175
Strazzullo, V., et al. 2006, A&A, 450, 909
Steidel, C. C., Adelberger, K. L., Shapley, A. E., Erb, D. K., Reddy, N. A., & Pettini, M. 2005, ApJ, 626, 44
Tanaka, M., Kodama, T., Arimoto, N., Okamura, S., Umetsu, K., Shimasaku, K., Tanaka, I., & Yamada, T. 2005, MNRAS, 362, 268
Thomas, D., Maraston, C., & Korn, A. 2004, MNRAS, 351, L19
Thomas, J., Saglia, R. P., Bender, R., et al. 2005, MNRAS, 360, 1355
Toft, S., Mainieri, V., Rosati, P., Lidman, C., Demarco, R., Nonino, M., & Stanford, S. A. 2004, A&A, 422, 29
Toft, S., et al. 2007, ApJ, 671, 285
Trager, S. C., Faber, S. M., Worthey, G., & González, J. J. 2000, AJ, 119, 1645
Treu, T., Stiavelli, M., Casertano, S., Møller, P., & Bertin, G. 1999, MNRAS, 308, 1037
Treu, T., Stiavelli, M., Bertin, G., Casertano, S., & Møller, P. 2001, MNRAS, 326, 237
Treu, T., Ellis, R. S., Liao, T. X., et al. 2005, ApJ, 633, 174
Trujillo, I., et al. 2004, ApJ, 604, 521
Trujillo, I., et al. 2006, ApJ, 650, 18
Trujillo, I., Conselice, C. J., Bundy, K., Cooper, M. C., Eisenhardt, P., & Ellis, R. S. 2007, MNRAS, 382, 109
van der Wel, A., Franx, M., van Dokkum, P. G., Rix, H.-W., Illingworth, G. D., & Rosati, P. 2005, ApJ, 631, 145

van der Wel, A., Franx, M., Wuyts, S., van Dokkum, P. G., Huang, J., Rix, H.-W., & Illingworth, G. D. 2006, ApJ, 652, 97
van Dokkum, P. G. & Franx, M. 1996, MNRAS, 281, 985
van Dokkum, P. G., Franx, M., Kelson, D. D., & Illingworth, G. D. 1998, ApJ, 504, L17+
van Dokkum, P. G., & Franx, M. 2001, ApJ, 553, 90
van Dokkum, P. G., & Stanford, S. A. 2003, ApJ, 585, 78
van Dokkum, P. G., & van der Marel, R. P. 2007, ApJ, 655, 30
Vanzella, E., et al. 2005, A&A, 434, 53
Vanzella, E., et al. 2006, A&A, 454, 423
Wolf, C., et al. 2004, A&A, 421, 913
Worthey, G. 1994, ApJS, 95, 107
Yi, S., Lee, Y.-W., Woo, J.-H., Park, J.-H., Demarque, P., & Oemler, A. J. 1999, ApJ, 513, 128
Yi, S., Demarque, P., & Oemler, A. J. 1997, ApJ, 486, 201
Zirm, A. W., et al. 2007, ApJ, 656, 66
Zirm, A. W., et al. 2008, ArXiv e-prints, 802, arXiv:0802.2095

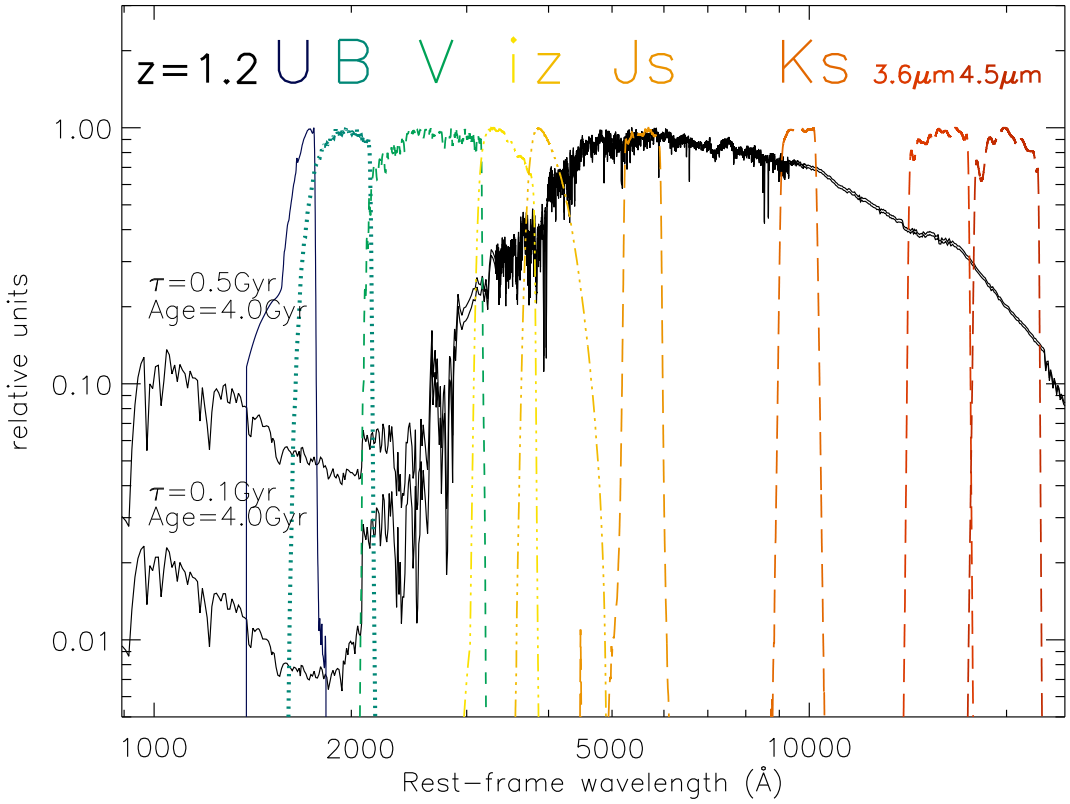

FIG. 1.— BC03 composite stellar population models of 4.0Gyr old models, of different τs. The colored lines are the filter transmission curves of the observing bands we use throughout this work, shifted to our sample rest-frame.

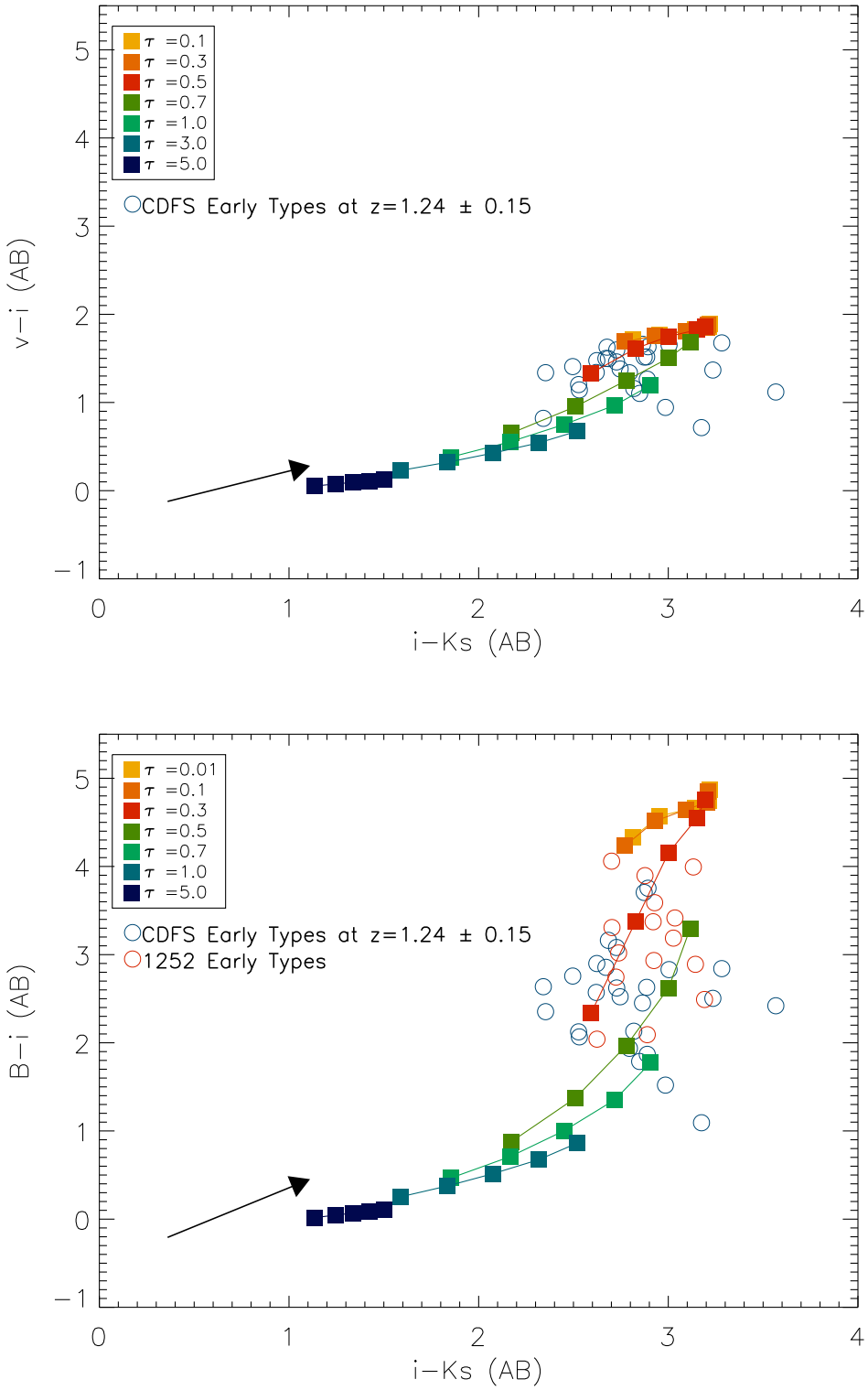

FIG. 2.— *Top panel*: $i - K_s$ vs $V - i$ color-color plot of $BC03$ composite stellar population models at $z = 1.24$ superimposed on our GOODS ETG photometry at $z = 1.24 \pm 0.15$ in blue circles. The squares account for SFHs with various τ models. The grids are drawn for seven different τs and five ages $(2, 2.5, 3, 3.5, 4$ Gyrs): the colored lines represent iso-metallicity colors of $Z_{\odot}$. The black arrow indicate an extinction of $E(B - V) = 0.2$ as parameterized with the reddening curve of (Cardelli et al. 1989). *Bottom left panel:* $i - K_s$ vs. $B - i$ color-color diagram of the same models and data: B-band ($\lambda_{rest} \sim 2000\AA$) is mandatory to break the age-SFH degeneracy at z=1.24

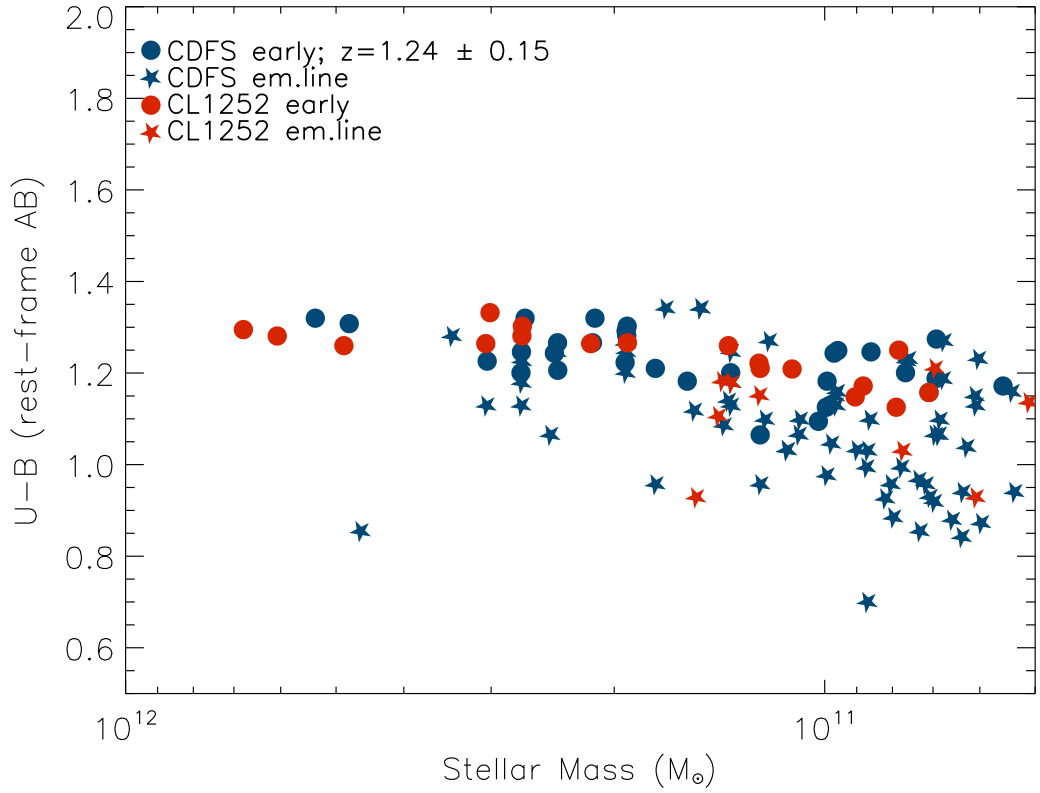

FIG. 3.— $U-B$ color - mass Diagram of the mass-selected samples of CL1252 early- (filled red circles) and late-type (red stars) galaxies as well as of CDFS field early- (filled blue circles) and late-type (blue stars) galaxies. Uncertainties in the stellar mass are ~ 0.15 dex. Field ETG galaxies are distributed around the cluster red-sequence, although with a larger scatter

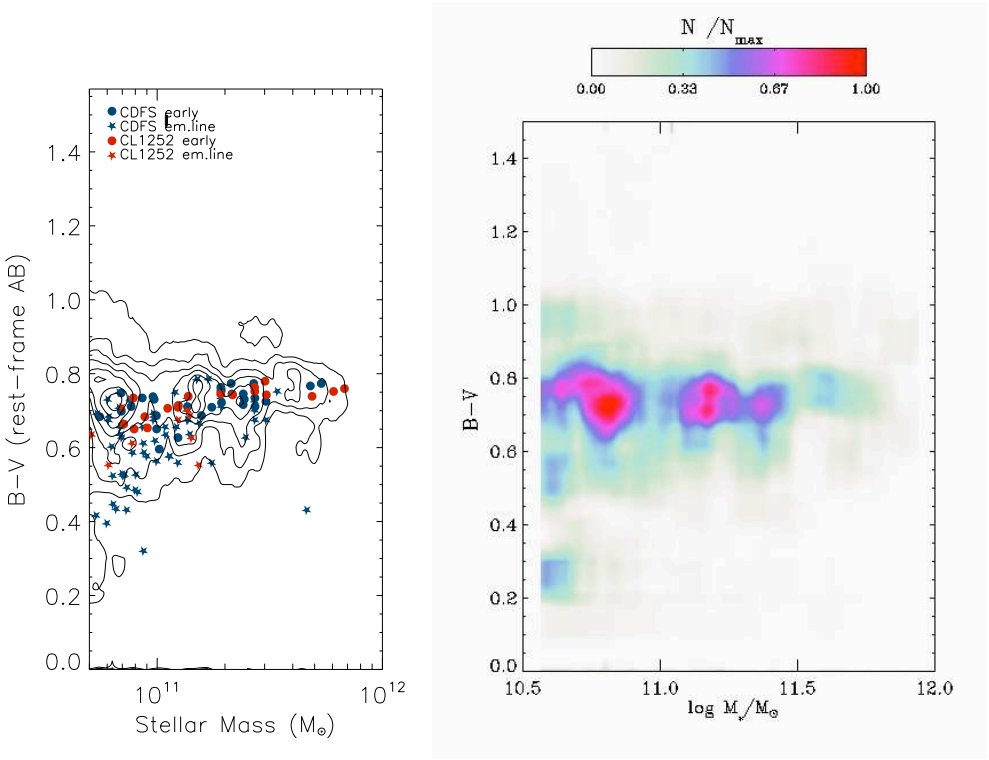

FIG. 4.— $B-V$ Color versus Stellar Mass diagram of the observed samples of cluster and field galaxies (*left panel*, symbols are the same as in Fig. 3) with over-plotted contours obtained with the models of Menci et al. (2008) (*right panel*) for galaxies in clusters; the color code represents the abundance of galaxies in a given $(\frac{logM_*}{M_\odot} - (B-V))$ bin.

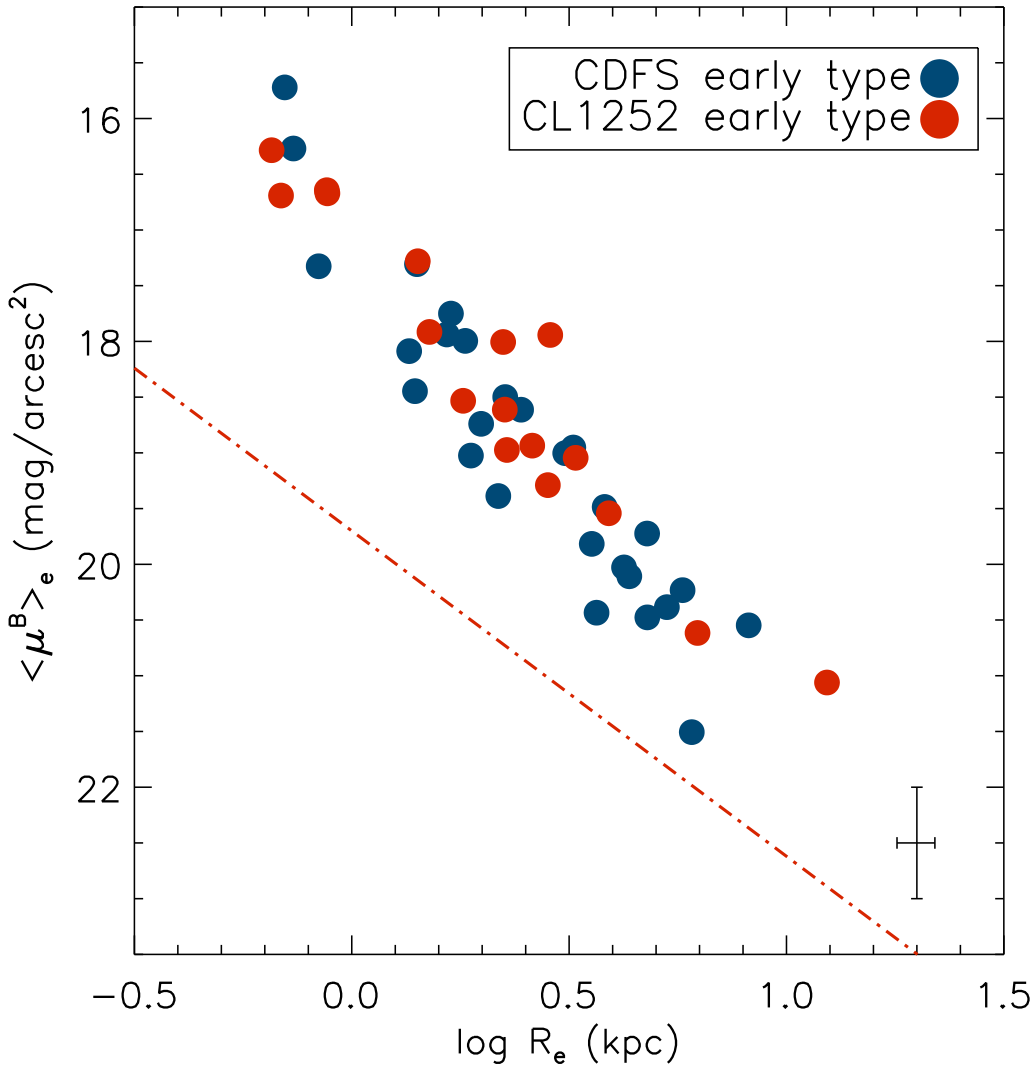

FIG. 5.— Mean surface brightness $< \mu_e >$ versus effective radius, $R_e[kpc]$. The Kormendy relation in the rest-frame B-band for our ETG in the field (filled blue circles) and in the cluster (filled red circles). All the data are corrected for the cosmological dimming $(1+z)^4$. The red dotted-dashed line represents the KR at $z \sim 0$ found by La Barbera et al. (2003), K-corrected to our rest-frame B-band. The error bar in the bottom-right is representative of the typical uncertainties of our measurements.

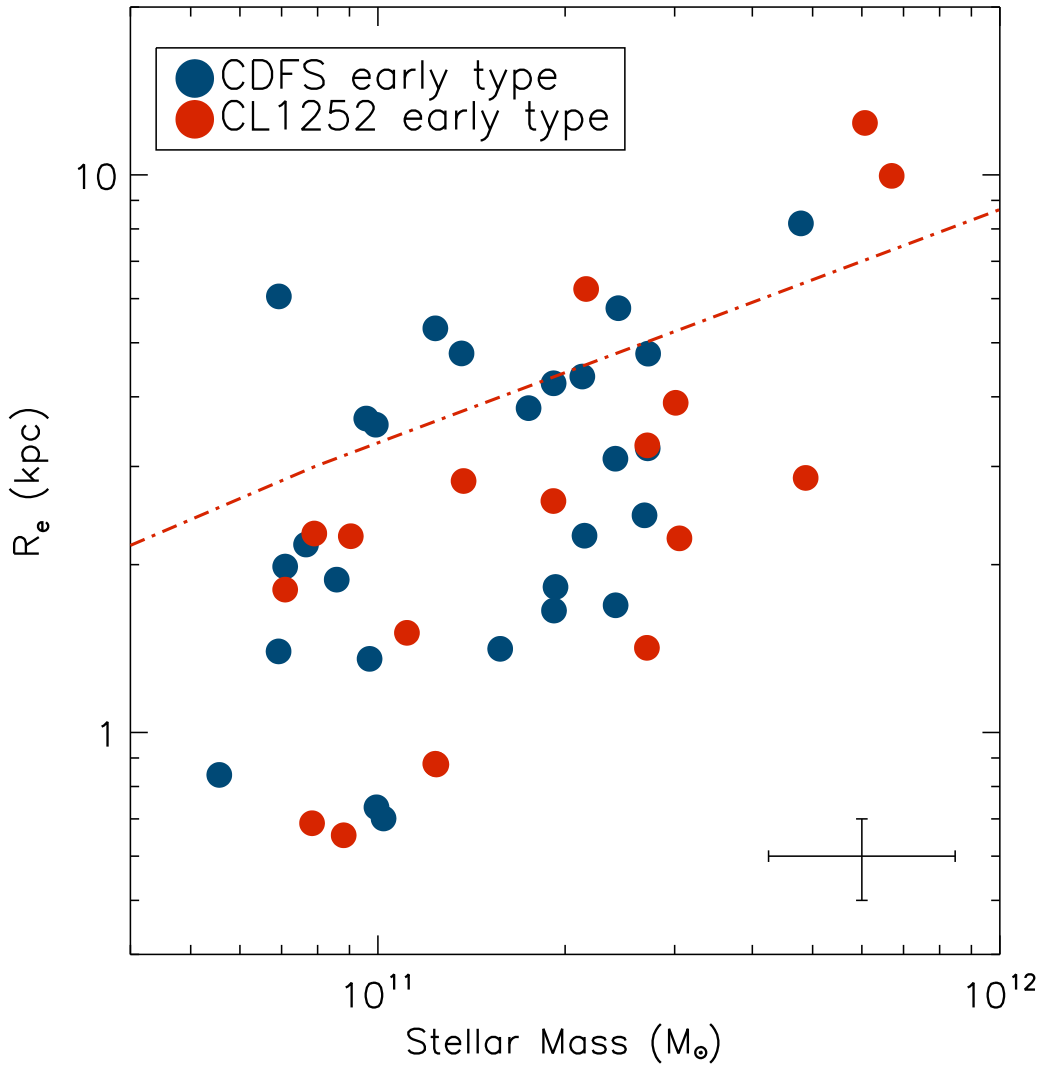

FIG. 6.— The stellar mass vs. size relation for the ETG in the cluster (filled red circles) and in the field (filled blue circles). The red dotted-dashed line represent the same relation at $z \sim 0$ found by (Shen et al. 2003) with SDSS data. The mean size relative error is $<$ 20%. Uncertainties in stellar mass are ~ 0.15 dex.

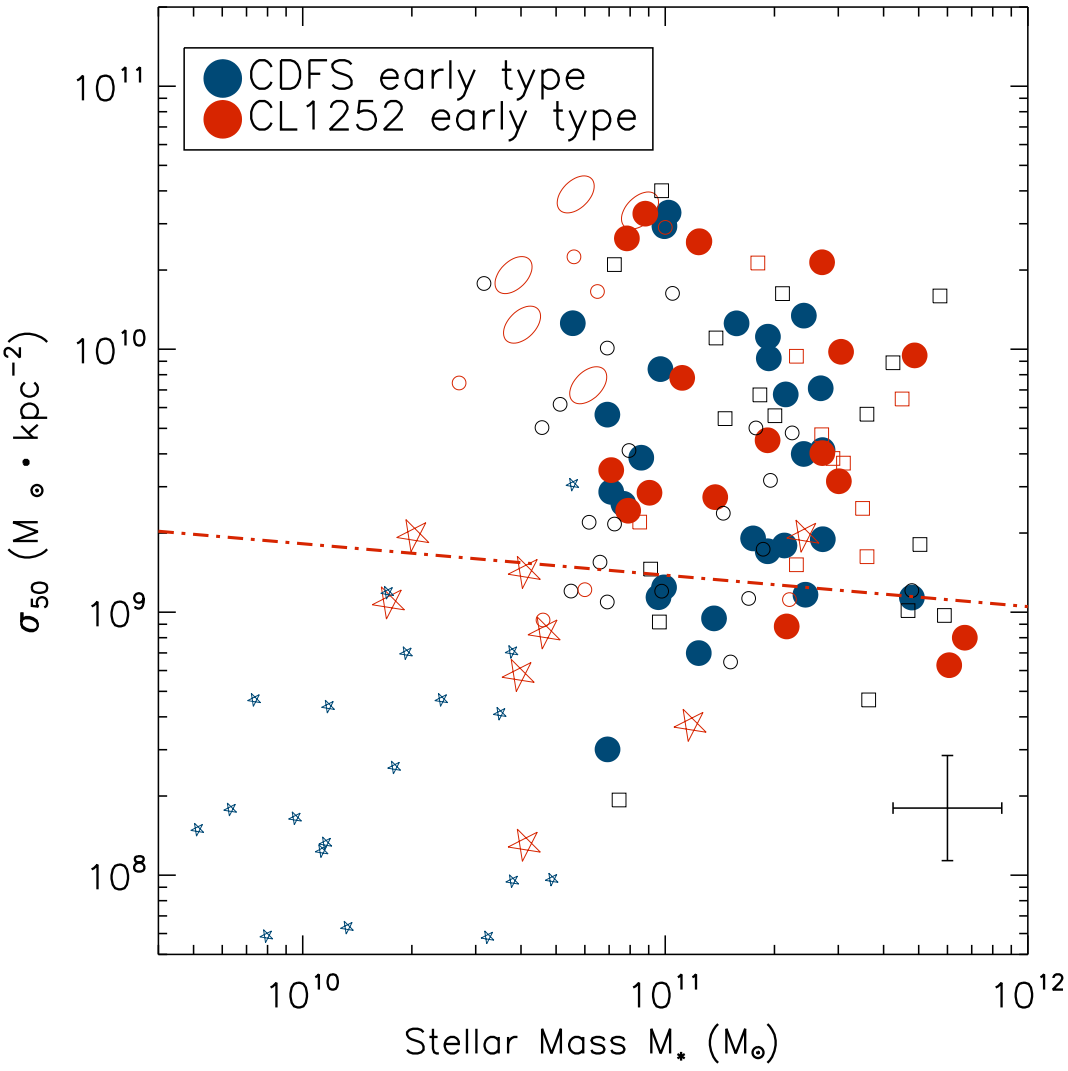

FIG. 7.— The stellar mass vs. the Average surface mass density within the half-light radius for the ETG in the cluster (filled red circles) and in the field (filled blue circles). For comparison we over-plot $z \sim 2.5$ quiescent DRGs (qDRGs) (open red ellipses), star-forming DRGs (sDRGs) (open red stars), LBGs (filled blue stars) from Zirm et al. (2007) paper. Other samples of $1.0 \lesssim z \lesssim 1.5$ ETG are also drawn from the works of (Trujillo et al. 2006) (open red squares), (Daddi et al. 2005) (open red circles), (van der Wel et al. 2006) (open black circles), and (Rettura et al. 2006) (open black squares). The red dotted-dashed line represent the local relation for ETG in SDSS calculated from the mass-size relation of Shen et al. (2003). The error bar in the bottom-right is representative of the typical uncertainties of our measurements.

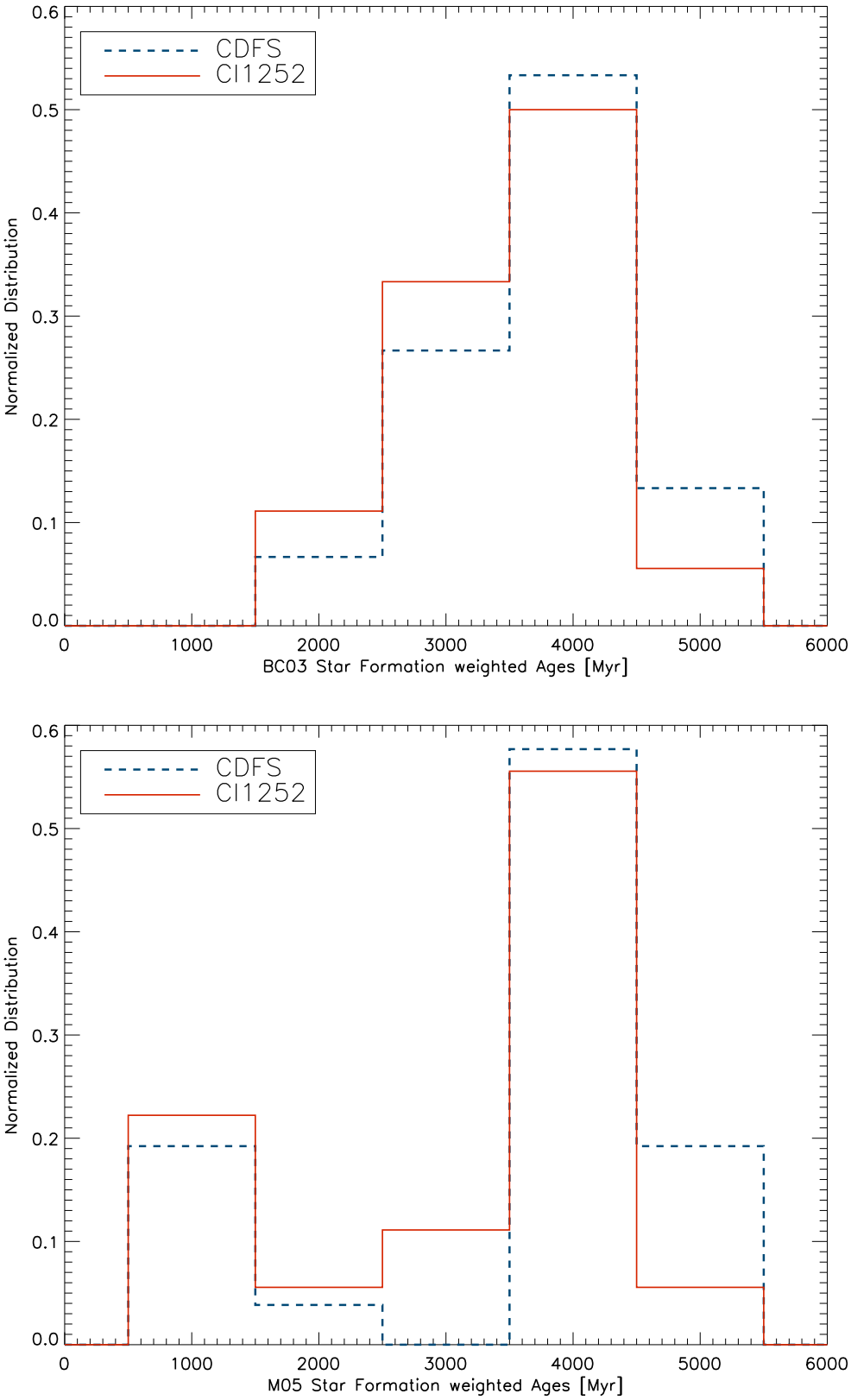

FIG. 8.— *Top panel*: Formation epochs of ETGs: Histogram of the field (dashed blue line) and cluster (solid red line) star-formation weighted ages derived with the BC03 models. *Bottom panel*: Histogram of the field and cluster star-formation-weighted ages derived with the M05 models.

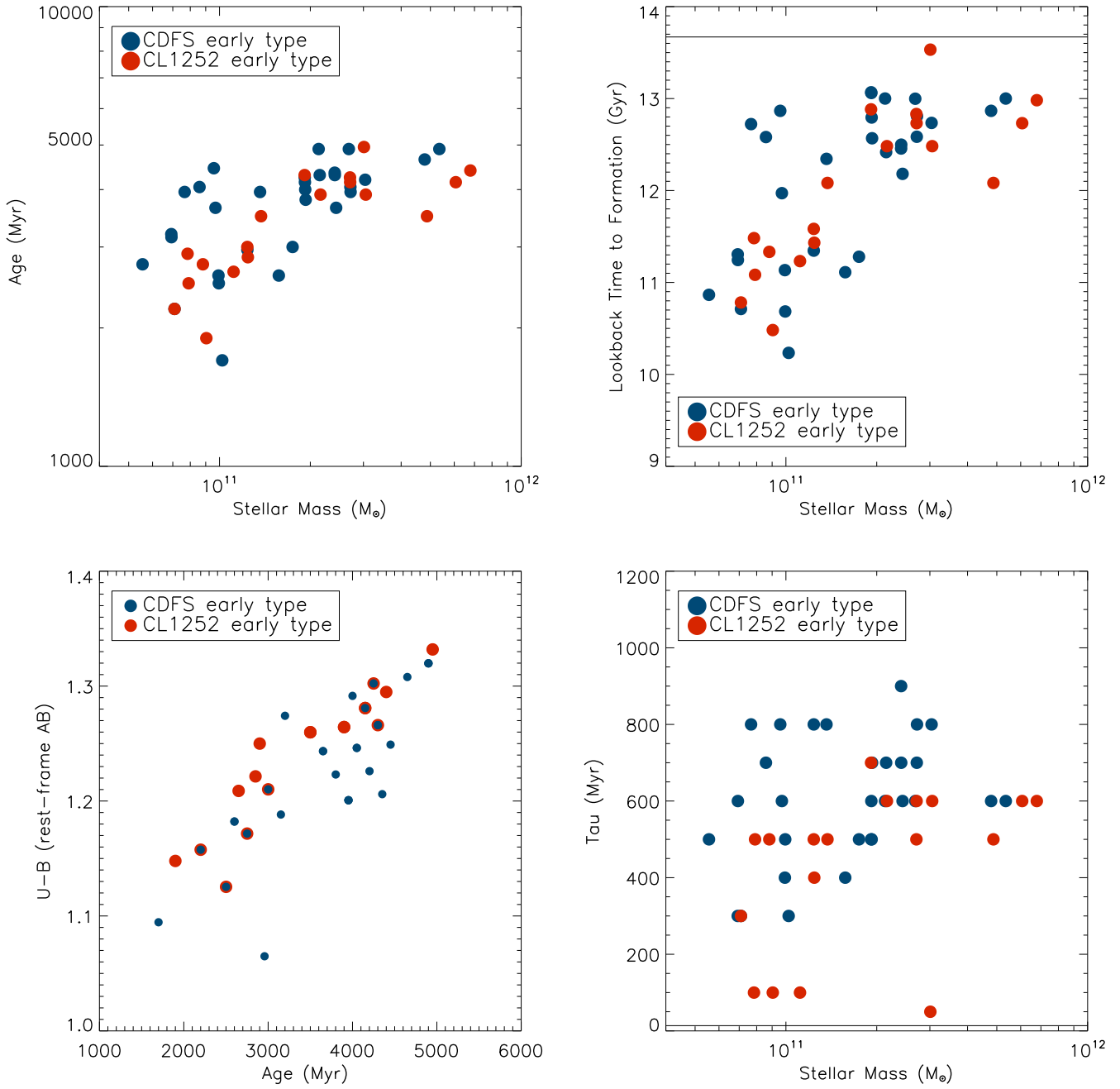

FIG. 9.— *Top-left panel*: Stellar mass vs. star formation weighted ages for the ETG in the cluster (filled red circles) and in the field (filled blue circles). *Top-right panel*: The dependence of the lookback time to formation on the galaxy mass. *Bottom-left panel*: Rest-frame $U-B$ color vs. age of ETG in both environments. *Bottom-right panel*: Formation *timescales*, τ, of ETG as a function of their stellar mass in both the field and cluster environment. The mean error in stellar age is 0.5 Gyr. Uncertainties in stellar masses and τ are ~ 0.15 dex and ~ 0.2 Gyr, respectively.

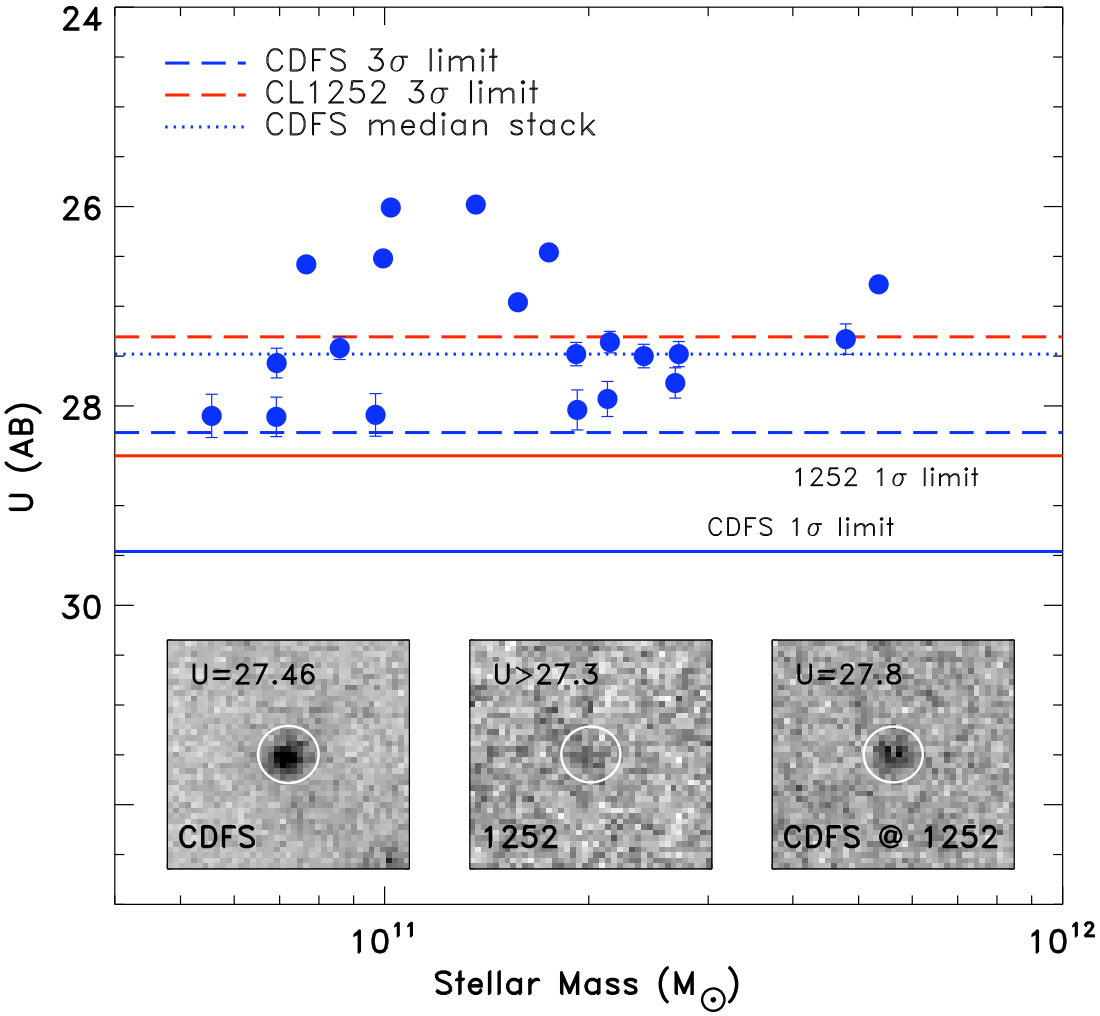

FIG. 10.— Stellar Mass vs. U-band observed magnitude (rest-frame $\sim 1700\AA$) for the ETG detected in the field (filled blue circles). Solid lines represent the 1σ (1" radius aperture) limiting magnitudes of our data-sets respectively (blue for the field, red for the cluster) Dashed lines represent the 3σ limits. The blue dotted line indicates the observed magnitude of the median stack of the field ETG U-band images. An image of the median stack of the field ETG U-band observations is displayed in the bottom-left corner. The median stack of the cluster ones is shown in the middle. The image at the bottom-right corner shows instead the CDFS stack, simulated in the actual CL1252 data. (see text for more details).

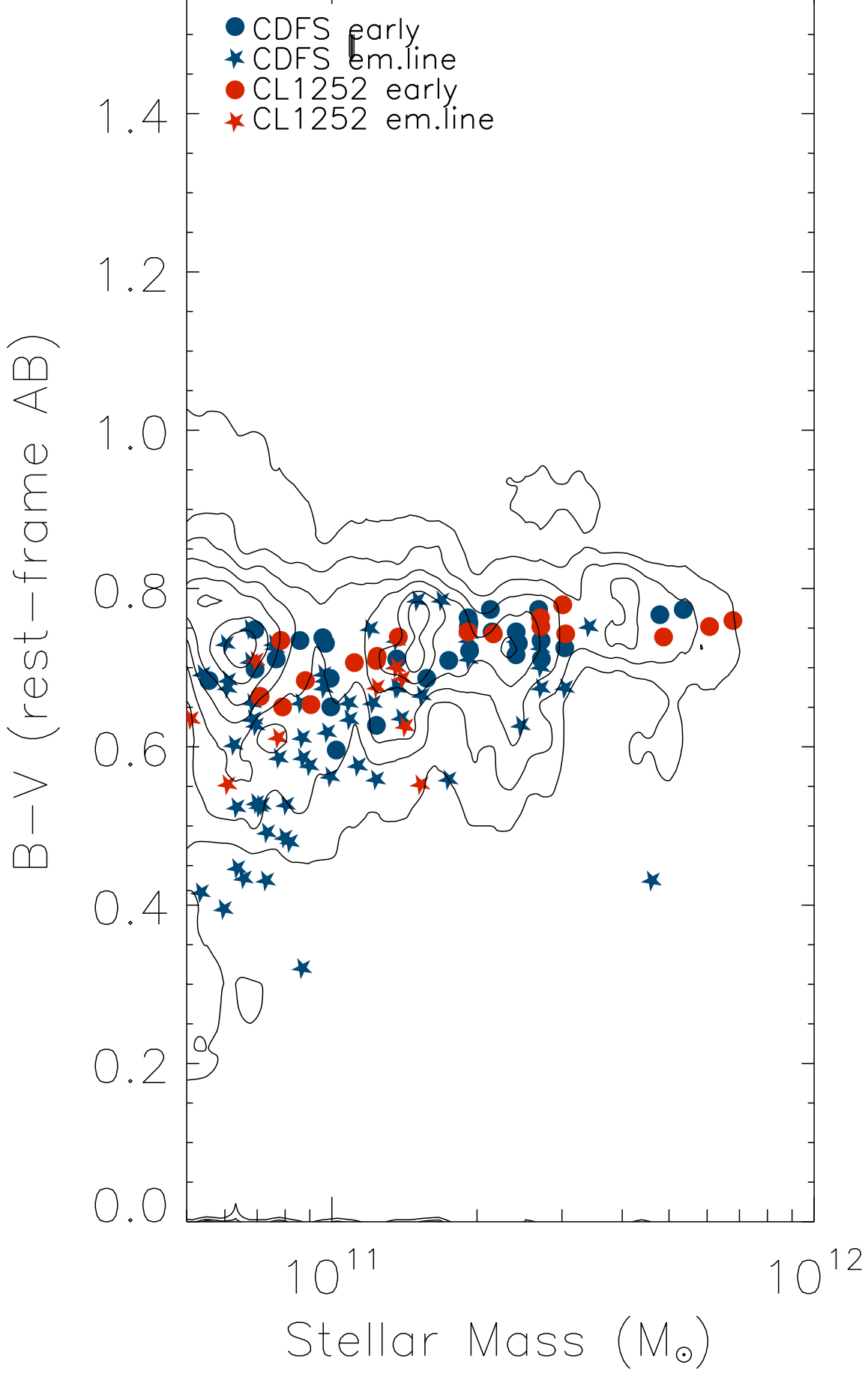
CDFS early
CDFS em.line
CL1252 early
CL1252 em.line
1.4
1.2
1.0
0.8
0.6
0.4
0.2
0.0
B−V (rest−frame AB)
10^{11}
10^{12}
Stellar Mass ($M_\odot$)